# **Green Chemistry**



#### **PAPER**

View Article Online
View Journal | View Issue



**Cite this:** *Green Chem.*, 2025, **27**, 13041

# Photoelectrochemical dicarboxylation of styrene with CO<sub>2</sub> to phenylsuccinic acid on a Ni-decorated silicon photocathode

Xiaoxue Zhou, <sup>a</sup> Hao Yang, <sup>b</sup> \*<sup>b,c</sup> Ziqi Zhao, <sup>a</sup> Hongxia Ning, <sup>a</sup> Yu Shan, <sup>a</sup> Ming Cheng, <sup>d</sup> Peili Zhang, <sup>a</sup> Fei Li, <sup>a</sup> Licheng Sun <sup>a</sup>, <sup>a</sup> and Fusheng Li <sup>b</sup> \*<sup>a,d</sup>

The conversion of CO<sub>2</sub> into value-added chemicals is highly critical for sustainable development. Among the various strategies, the dicarboxylation of alkenes with CO<sub>2</sub> offers a highly attractive route to access synthetically valuable dicarboxylic acids, which serve as key intermediates in the production of polymers and pharmaceuticals. Photoelectrochemical (PEC) carboxylation represents an efficient and sustainable carboxylation strategy, offering distinct advantages including mild reaction conditions, cost-effectiveness, and environmental compatibility. In this study, an efficient PEC system is presented for the carboxylation of styrene using a Ni-modified p-type micro-pyramid silicon (Ni/p-Si) photocathode. The incorporation of the Ni catalyst significantly suppresses charge recombination and accelerates charge transfer at the electrode-electrolyte interface, thereby enhancing the overall photoelectrochemical performance. The optimized Ni/p-Si photocathode achieved 77.7% faradaic efficiency (FE) for phenylsuccinic acid at -2.4 V vs. Aq/AqCl, with a photocurrent density of -4.5 mA cm<sup>-2</sup>. Moreover, this PEC platform demonstrates moderate FEs across a range of substituted styrenes, indicating good functional group tolerance. Mechanistic studies reveal that the reaction proceeds via single-electron reduction of styrene to generate radical anions, which undergo CO2 addition followed by further reduction and subsequent attack on a second CO<sub>2</sub> molecule to yield succinic acid. These findings broaden the scope of CO<sub>2</sub> utilization through selective and sustainable C-C bond formation processes.

Received 20th July 2025, Accepted 11th September 2025 DOI: 10.1039/d5qc03730a

rsc.li/greenchem

#### **Green foundation**

- 1. This work advances green chemistry by developing a sacrificial-anode-free photoelectrochemical (PEC) system that enables the direct dicarboxylation of alkenes with CO<sub>2</sub> under mild conditions, offering a sustainable route to access valuable dicarboxylic acids.
- 2. The Ni/p-Si photocathode achieves a faradaic efficiency of 77.7% toward phenylsuccinic acid without sacrificial metals or toxic reagents. It exhibits a broad substrate scope, reduced energy input, and enhanced charge separation, minimizing waste and improving atom economy.
- 3. The greenness of this system could be further enhanced by integrating Earth-abundant, fully recyclable cocatalysts and coupling PEC processes with solar-driven anodic oxidation to eliminate the need for external bias, moving toward fully self-sustained artificial photosynthesis.

#### <sup>a</sup>State Key Laboratory of Fine Chemicals, Frontier Science Center for Smart Materials, School of Chemical Engineering, Dalian University of Technology, 116024 Dalian, Liaoning, China. E-mail: lifusheng.fshy@sinopec.com

#### Introduction

Carbon dioxide (CO<sub>2</sub>) is widely regarded not only as a notorious greenhouse gas but also as an inexpensive, abundant, nontoxic, and ideal C1 building block.<sup>1–3</sup> The utilization and conversion of CO<sub>2</sub> into value-added chemicals have been recognized as promising ways to mitigate energy shortages and environmental problems caused by the greenhouse effect.<sup>4</sup> Beyond its direct reduction to small-molecule fuels,<sup>5,6</sup> the incorporation of CO<sub>2</sub> into organic molecules (such as ketones,<sup>7</sup> alkynes,<sup>8</sup> alkenes,<sup>9</sup> and alkyl halides<sup>10</sup>) enables the synthesis of carboxylic acids, which are critical ingredients for the synthesis of pharmaceuticals, cosmetics, pesticides, dyes,

<sup>&</sup>lt;sup>b</sup>Leiden Institute of Chemistry, Leiden University, P. O. Box 9502, 2300 RA Leiden, The Netherlands. E-mail: h.yang@lic.leidenuniv.nl

<sup>&</sup>lt;sup>c</sup>Department of Chemistry, School of Engineering Sciences in Chemistry, Biotechnology and Health, KTH Royal Institute of Technology, 10044 Stockholm, Sweden

<sup>&</sup>lt;sup>d</sup>SINOPEC (Dalian) Research Institute of Petroleum and Petrochemicals Co. Ltd, 116045 Dalian Lianning China

<sup>&</sup>lt;sup>e</sup>Center of Artificial Photosynthesis for Solar Fuels and Department of Chemistry, School of Science, Westlake University, 310024 Hangzhou, China

and other highly valuable chemicals.  $^{11,12}$  Among these substrates, alkenes have attracted particular attention due to their wide availability and structural diversity.  $^{13}$  The carboxylation of alkenes with  $\rm CO_2$  enables direct access to structurally diverse carboxylic acids, avoiding conventional multistep formylation/oxidation processes.  $^{14}$  This approach represents an efficient and sustainable carboxylation strategy, offering distinct advantages including mild reaction conditions, cost-effectiveness, and environmental benignity for green chemical synthesis.  $^{12}$ 

Significant efforts have been made to achieve the carboxylation of alkenes with CO2 through traditional transition-metal catalysis, electrochemical, photocatalysis, and photoelectrocatalysis methods. 15-20 Among these methods, photoelectrochemical (PEC) catalysis, combining the advantages of both photocatalysis and electrocatalysis, offers a compelling platform for converting and storing solar energy in chemical substances under mild conditions. 21,22 Specifically, PEC carboxylation directly utilizes solar energy to generate electron-hole pairs over electrocatalysis, which effectively reduces the overpotential and enhances the energy conversion efficiency, enabling carboxylation reactions to proceed under milder potentials with higher energy efficiency and superior selectivity.<sup>23</sup> The successful implementation of PEC carboxylation of alkenes with CO2 critically depends on the rational design and fabrication of the photocathode. Silicon (Si) stands out as one of the most promising semiconductor materials for photocathode applications, owing to its Earth abundance, narrow band gap (1.12 eV) with efficient light harvesting, low cost, high carrier mobility, and streamlined large-scale production. 24-26

Silicon photocathodes have emerged as particularly promising materials for PEC applications, demonstrating excellent performance in both the PEC hydrogen evolution and CO<sub>2</sub> reduction reactions.<sup>27,28</sup> Notably, PEC hydrocarboxylation with CO<sub>2</sub> as a substrate was first achieved using a silicon-nanowire

(SiNW) photocathode with a sacrificial Al anode, enabling the synthesis of α-hydroxy acids from aromatic ketones.<sup>29</sup> This approach was successfully extended to α,β-unsaturated ketones using unmodified SiNWs. 30 While these studies established the viability of light-driven PEC hydrocarboxylation, the reaction efficiency remained fundamentally constrained by the limited catalytic activity of bare Si. To enhance the reaction kinetics, a homogeneous nickel-based molecule was subsequently employed in the PEC carboxylation system, 31 which improved the reaction kinetics but introduced new challenges, including metal toxicity, difficult product separation, and low catalyst utilization efficiency. As alternatives, heterogeneous catalyst-modified photoelectrodes have shown great potential. For instance, a recent study demonstrated that a Ag nanoparticle-decorated Si photocathode paired with an Al sacrificial anode enabled selective CO2 fixation for the synthesis of a profen drug intermediate.<sup>32</sup> Despite these advances, the development of highly selective, broadly applicable catalyst-modified photocathodes, particularly in nonsacrificial metal PEC systems, remains an unmet challenge in PEC carboxylation. Moreover, the use of silicon-based PEC platforms for alkene dicarboxylation has been largely unexplored, highlighting a critical gap in current CO2 valorization strategies.

In this study, we demonstrate an efficient and nonsacrificial PEC system for the dicarboxylation of styrene with CO<sub>2</sub>, utilizing a Ni-modified micro-pyramidal Si photocathode (Ni/p-Si) in conjunction with a graphite anode (Fig. 1). The rationally designed micro-pyramid array architecture simultaneously suppresses optical reflectance and enhances photon capture efficiency. The incorporation of a Ni cocatalyst significantly improves the PEC performance by effectively suppressing electron-hole recombination and significantly promoting interfacial charge transfer, resulting in a remarkable enhancement of photocurrent. The Ni/p-Si photocathode achieves a maximum faradaic efficiency (FE) of 77.7% for the reductive dicarboxylation of styrene to phenyl-

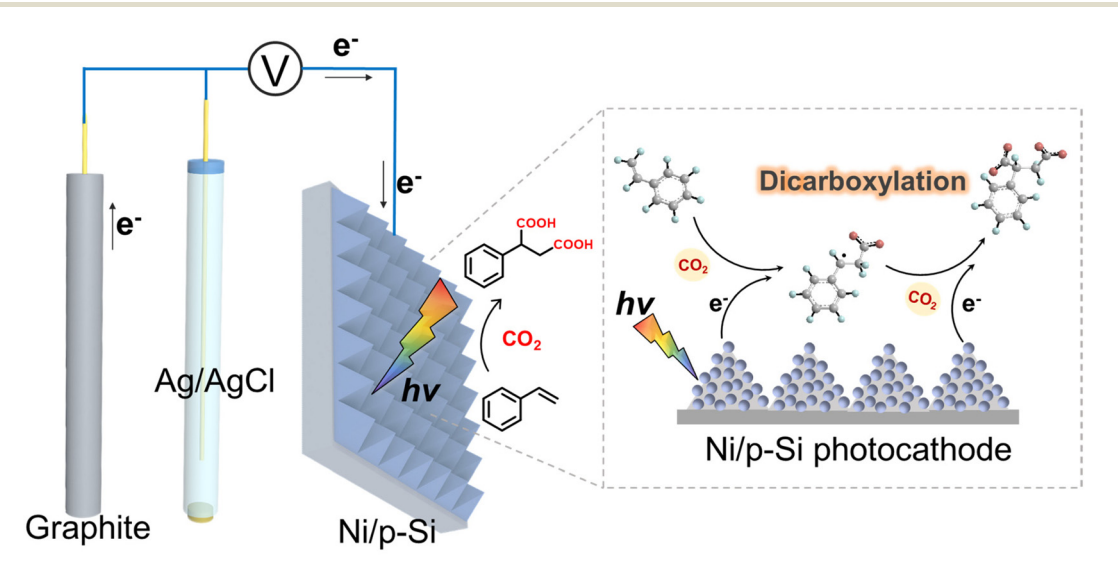


Fig. 1 Schematic diagram of PEC dicarboxylation on the Ni/p-Si photocathode.

**Green Chemistry** Paper

succinic acid at -2.4 V vs. Ag/AgCl. Moreover, this photocathode exhibits broad substrate tolerance, delivering FEs ranging from 43.6% to 65.8% across a series of electronically diverse styrene derivatives, including both electron-rich and electron-deficient substrates, as well as trans-stilbene. This study establishes a catalyst-modified silicon photocathode as a robust and highly efficient platform for PEC dicarboxylation, providing an economical and scalable route to access value-added succinic acid derivatives from CO2 and simple alkenes.

#### Results and discussion

The preparation of the Ni/p-Si photocathode is schematically illustrated in Fig. 2a. The planar p-type silicon wafer was structured by a rapid anisotropic etching treatment to generate a light-trapping micro-pyramidal structure on the surface.<sup>33</sup> Subsequently, the Ni catalyst was decorated on the p-Si by photoelectrodeposition. The surface morphologies of the p-Si and Ni/p-Si electrodes were characterized by scanning electron microscopy (SEM). The SEM images of the etched p-Si substrate reveal a densely packed array of micro-pyramidal structures with a polydisperse size distribution, uniformly covering the silicon surface (Fig. S1).

The SEM images shown in Fig. 2b and Fig. S2 confirm the successful deposition of the Ni catalyst on the surface of the p-Si substrate, clearly revealing a uniform distribution of the

Ni catalyst with an average size of approximately 100 nm. The elemental mappings and energy-dispersive X-ray (EDX) spectroscopy (Fig. S3) further reveal a uniform distribution of Ni across the photocathode surface. The surface composition and chemical states of the as-prepared Ni/p-Si were analyzed by X-ray photoelectron spectroscopy (XPS) (Fig. S4a), confirming the presence of Ni on the silicon surface. The high-resolution XPS spectrum of the Ni 2p region for Ni/p-Si (Fig. 2c) reveals that the deposited nickel catalyst is composed of both metallic Ni and Ni<sup>2+</sup> species. The peaks with binding energies of 852.5 and 869.7 eV correspond to Ni 2p<sub>3/2</sub> and Ni 2p<sub>1/2</sub> of metallic nickel, respectively, while the peaks at 855.5 and 873.3 eV are attributed to the Ni<sup>2+</sup> species. 34,35 Additionally, the Si 2p spectrum indicates the presence of a thin layer of silicon dioxide on the surface (Fig. S4b). X-ray diffraction (XRD) analysis shows no discernible diffraction peaks for Ni (Fig. S5), suggesting that the deposited nickel catalyst is amorphous.

Following the successful fabrication and structural characterization of the Ni/p-Si photocathode, its photoelectrochemical carboxylation performance was evaluated using styrene as a model substrate. To investigate the influence of the styrene concentration, PEC carboxylation reactions were conducted with varying initial concentrations of styrene in CO2-saturated 0.1 M tetrabutylammonium bromide (TBAB) anhydrous acetonitrile solutions. Linear sweep voltammetry (LSV) scans were recorded at a scan rate of 20 mV s<sup>-1</sup> under simulated 1-sun illumination (100 mW cm<sup>-2</sup>), without IR compensation. Styrene concen-

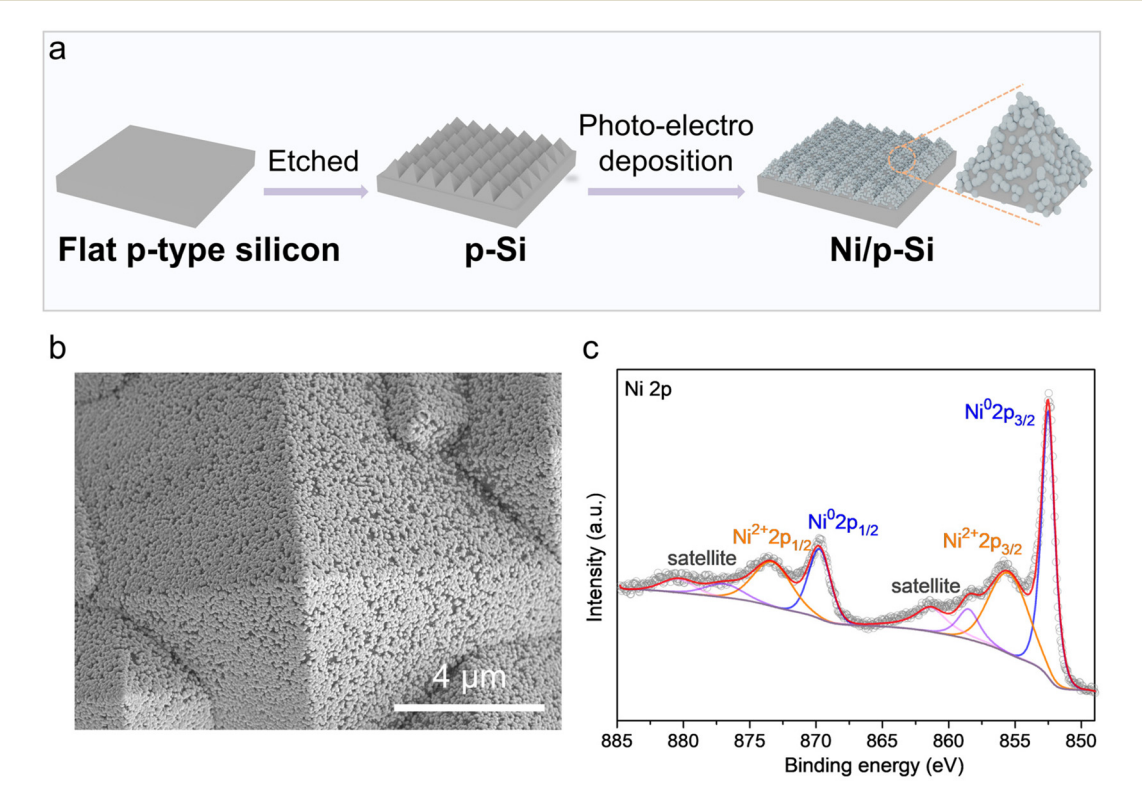


Fig. 2 (a) Schematic illustration of the preparation process for Ni/p-Si. (b) SEM image of Ni/p-Si. (c) High-resolution XPS spectrum of the Ni 2p region for the as-fabricated Ni/p-Si electrode.

trations ranging from 0 to 0.2 M were examined. As shown in Fig. S6, the photocurrent density increased significantly with increasing styrene concentration up to 0.1 M, indicating enhanced electron consumption by substrate availability. Beyond this concentration, the photocurrent reached a saturation plateau as the mass transfer limitation was eliminated. Therefore, 0.1 M was selected as the optimal styrene concentration for subsequent PEC dicarboxylation studies.

The performance of PEC carboxylation on the Ni/p-Si photocathode was evaluated in a three-electrode single cell. The electrolyte was composed of 10 mL of CO<sub>2</sub>-saturated acetonitrile solution containing 0.1 M styrene and TBAB. As shown in Fig. 3a, a relatively low photocurrent density was observed in the CO<sub>2</sub>-saturated electrolyte without styrene, indicating limited PEC CO<sub>2</sub> reduction activity under these conditions. In contrast, the introduction of 0.1 M styrene under an Ar atmosphere generated an apparent photocurrent response, predominantly attributed to radical polymerization under anhydrous conditions.<sup>36</sup> Remarkably, when both CO<sub>2</sub> and styrene were present, the photocurrent density increased significantly, accompanied by a notable positive shift in the onset potential. These results strongly suggest that the carboxylation reaction is initiated only when both reactants are simultaneously available, consistent with the proposed reaction precesses.<sup>12</sup>

The effect of applied potential on the PEC carboxylation performance of the Ni/p-Si photocathode was systematically investigated. Two primary liquid-phase products were identified: phenylsuccinic acid (2COOH, dicarboxylation product) hydrocinnamic acid (1COOH, hydrocarboxylation product). Reversed-phase high-performance liquid chromatography (HPLC) was employed for qualitative and quantitative analyses of both products (Fig. S7), with retention times of 4.5 min for **2COOH** and 8.3 min for **1COOH**, respectively. <sup>37,38</sup> Chronoamperometric measurements were conducted at different applied potentials, followed by acidification with 2 M HCl to protonate carboxylate intermediates prior to product extraction and detection (Fig. S8). The corresponding FEs, selectivity and average yield rates were calculated according to eqn (S1)-(S3) in the SI. As shown in Fig. 3b, the optimal applied potential for the production of 2COOH was found to be -2.4 V vs. Ag/AgCl with a remarkable FE as high as 77.7  $\pm$ 1.0%. Notably, the carboxylation reaction achieved an overall FE of 90%, confirming the viability of this PEC carboxylation strategy rather than the reduction of CO<sub>2</sub> or styrene alone. The selectivity of **2COOH** on Ni/p-Si was 79.4  $\pm$  1.7% at -2.4 V  $\nu s$ . Ag/AgCl (Fig. S9). As illustrated in Fig. 3c, the production rate of 2COOH showed a clear potential dependence, with the yield rate progressively increasing at more negative potentials. The

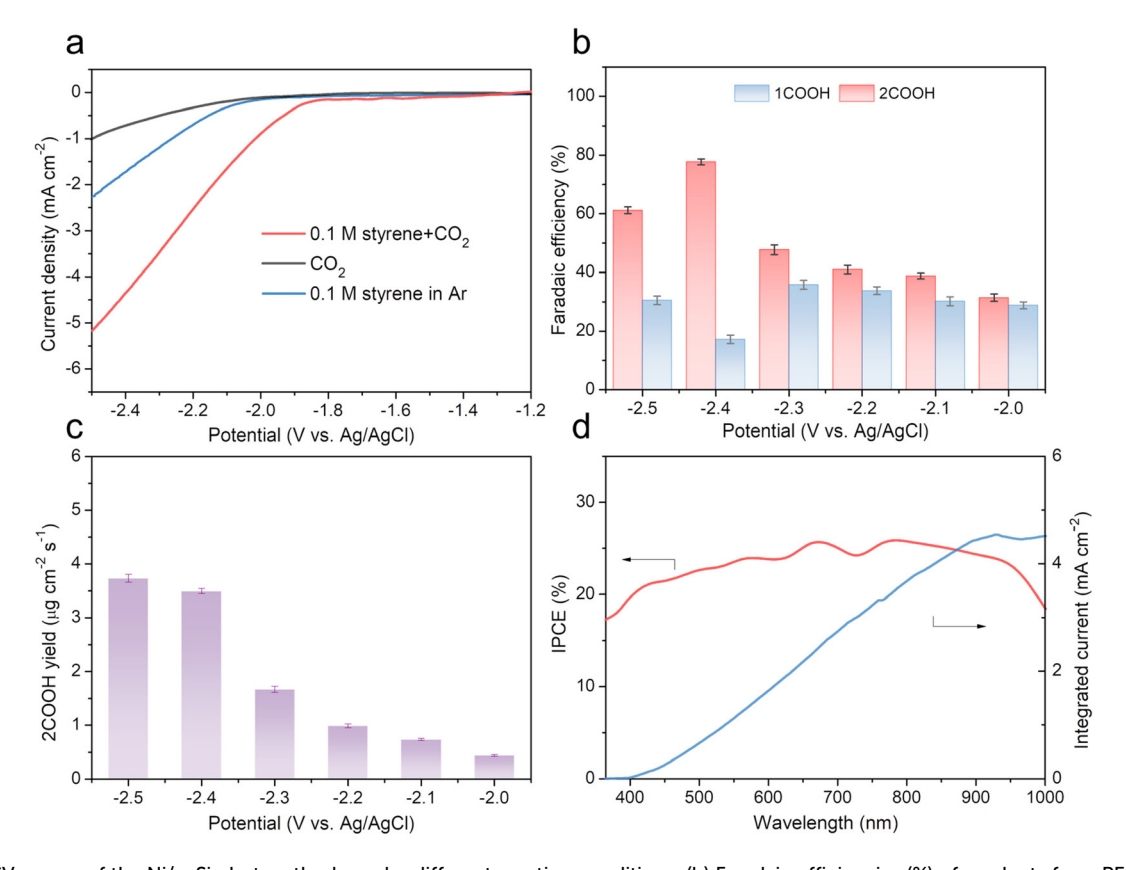


Fig. 3 (a) LSV curves of the Ni/p-Si photocathode under different reaction conditions. (b) Faradaic efficiencies (%) of products from PEC carboxylation of styrene under different potentials. (c) Yield rates of 2COOH production for Ni/p-Si at different applied potentials. (d) IPCE of the Ni/p-Si photocathode at -2.4 V vs. Ag/AgCl under monochromatic light at different wavelengths.

Ni/p-Si photocathode attained a maximum **2COOH** production rate of  $3.7 \pm 0.1 \,\mu g \, cm^{-2} \, s^{-1}$  at  $-2.5 \, V \, \nu s$ . Ag/AgCl.

**Green Chemistry** 

The incident-photon-to-current efficiency (IPCE) of the Ni/p-Si photocathode was measured under monochromatic light irradiation at an applied potential of  $-2.4~V~\nu s$ . Ag/AgCl (Fig. 3d). The Ni/p-Si photocathode reached a maximum IPCE of 25.6% at 670 nm. In addition, by integrating the IPCE curve over the AM 1.5G solar irradiation (ASTM G173-03) spectrum, a photocurrent of 4.5 mA cm $^{-2}$  at  $-2.4~V~\nu s$ . Ag/AgCl was obtained, which was consistent with the measured LSV curve photocurrent value, confirming the consistency and reliability of the PEC performance data.

These findings further prompted an investigation into the role of the Ni cocatalyst in enhancing the PEC performance of the microstructured silicon electrode. As shown in Fig. 4a, the PEC carboxylation activity of planar Si, etched p-Si, and Ni/p-Si photocathodes was systematically compared. The planar Si photocathode presented a negligible photocurrent due to its high surface reflectivity, resulting in poor intrinsic catalytic activity. <sup>39,40</sup> In contrast, the p-Si photocathode demonstrated a significantly enhanced photocurrent response, which can be attributed to the improved light-harvesting capability of the micro-pyramidal surface structure (Fig. S10). This result high-

lights the importance of morphological engineering in promoting PEC performance. Remarkably, the Ni/p-Si photocathode exhibited the most positive onset potential (-1.9 V vs. Ag/AgCl) and the highest photocurrent density for the PEC carboxylation of styrene with CO<sub>2</sub>. These enhancements are attributed to the accelerated interfacial charge-transfer kinetics facilitated by the Ni cocatalyst. Furthermore, the onset potential for styrene carboxylation on the Ni/p-Si photocathode showed a positive shift of approximately 0.5 V compared to that observed on a glassy carbon electrode (Fig. S11), highlighting the catalytic superiority and synergistic effect of the PEC system.

Further insight into the photoelectrochemical behavior was obtained by analyzing the transient photocurrent responses of the p-Si and Ni/p-Si photocathodes at a constant bias of -2.4 V vs. Ag/AgCl (Fig. 4b). The Ni/p-Si photocathode achieved a remarkably enhanced photocurrent density of -4.5 mA cm<sup>-2</sup>, representing a four-fold enhancement compared to that of the bare p-Si photoanode. Additionally, the Ni/p-Si photocathode presented much smaller transient spikes than the p-Si electrode during each on-off cycle, suggesting more efficient charge transfer and reduced charge recombination facilitated by the Ni cocatalyst. <sup>41</sup> To further evaluate the interfacial photo-

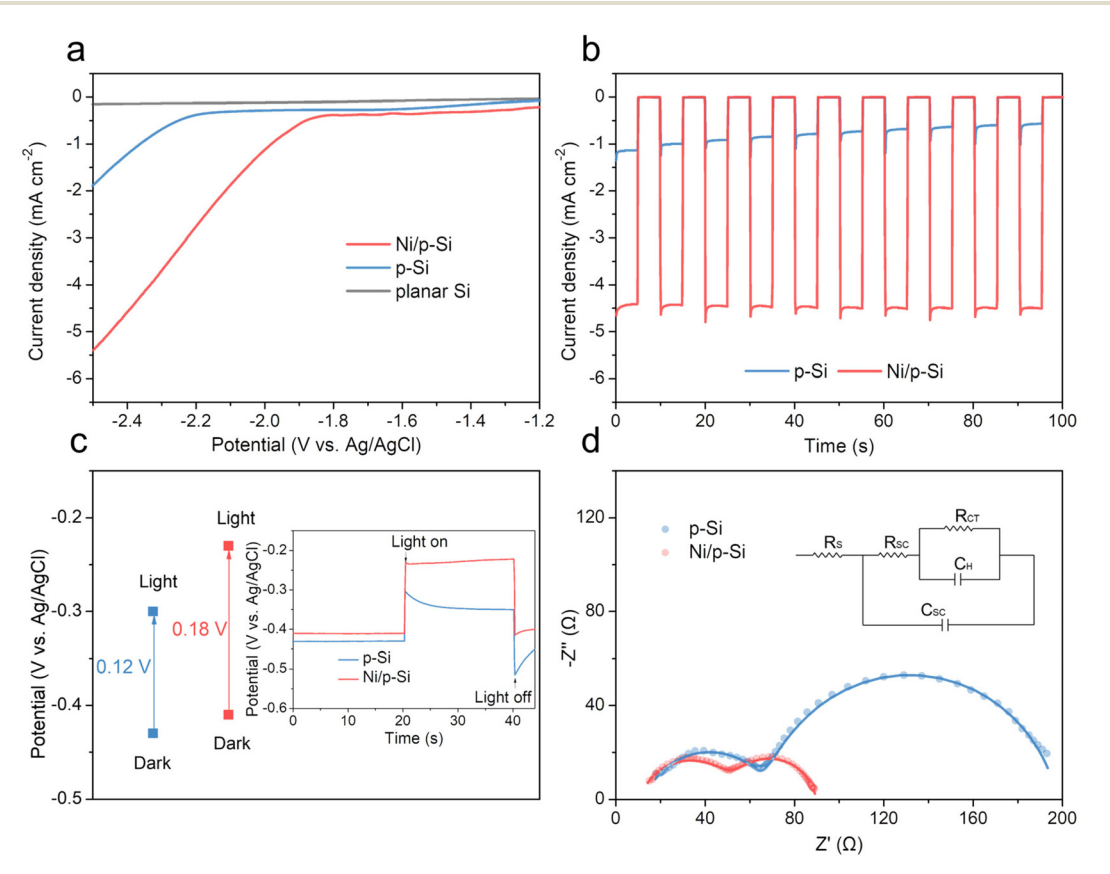


Fig. 4 (a) LSV curves of the planar Si, p-Si, and Ni/p-Si photocathodes in a  $CO_2$ -saturated 0.1 M tetrabutylammonium bromide (TBAB) acetonitrile solution containing 0.1 M styrene under AM 1.5 G illumination (100 mW cm<sup>-2</sup>). (b) I-t curves of the p-Si and Ni/p-Si photocathodes under chopped illumination at -2.4 V vs. Ag/AgCl. (c) Open-circuit potential (OCP) measurements of p-Si and Ni/p-Si under dark and light conditions. (d) Nyquist plots of p-Si and Ni/p-Si at -2.4 V vs. Ag/AgCl under light. Inset: corresponding equivalent circuit model.

response, the photovoltage  $(V_{\rm ph})$  at the photocathode/electrolyte interface was determined from the open-circuit potential (OCP) difference between illuminated and dark conditions (Fig. 4c). The Ni/p-Si photocathode exhibited an increased photovoltage of 0.18 V, compared to 0.12 V for p-Si, demonstrating that the Ni catalyst enhanced the interfacial electric field. This strengthened band bending at the semiconductor/electrolyte interface promoted charge separation and suppressed recombination, thereby contributing to the observed improvements in both onset potential and photocurrent density.  $^{42,43}$ 

To gain further insights into the charge transfer behavior, photoelectrochemical impedance spectroscopy measurements were conducted to investigate charge transfer kinetics across the semiconductor/catalyst/electrolyte interfaces. The PEIS responses of the bare p-Si and Ni/p-Si photocathodes at -2.4 vs. Ag/AgCl under illumination are displayed in Fig. 4d. The resulting Nyquist plots exhibit two well-defined semicircle features, which were fitted using a resistor-capacitor equivalent circuit model (inset, Fig. 4d). In this model, R<sub>s</sub> corresponds to the series resistance of the circuit, modeling the Cu substrate and Si semiconductor interface at high frequencies.  $R_{sc}$  represents the bulk resistance between the Si and Ni catalyst, while  $C_{\rm sc}$  accounts for the capacitive behavior of the electrodes. Additionally, the surface-state capacitance  $(C_{\rm H})$  and charge-transfer resistance  $(R_{\rm ct})$  at the electrode/electrolyte interface reflect the properties of the Helmholtz layer. 44,45 The fitted parameters derived from this model are summarized in Table S1. Compared to the bare p-Si electrode, the Ni/p-Si electrode displays significantly smaller semicircle diameters, indicating lower interfacial resistances. Specifically, the Ni/p-Si electrode demonstrates significantly reduced resistances ( $R_{\rm sc}$  = 44.48  $\Omega$ ,  $R_{\rm ct}$  = 34.53  $\Omega$ ) compared to bare p-Si ( $R_{\rm sc}$ = 56.35  $\Omega$ ,  $R_{\rm ct}$  = 128.50  $\Omega$ ). These reductions confirm enhanced bulk charge transport and accelerated charge transfer facilitated by the Ni catalyst, consistent with the electrochemical performance trends observed in LSV measurements (Fig. 4a). In summary, the Ni catalyst serves as highly efficient catalytic sites for the CO2 carboxylation reaction, promoting efficient separation of photogenerated charge carriers and enhancing charge transfer across the electrode/electrolyte interface, thereby significantly enhancing the PEC carboxylation efficiency observed in the Ni/p-Si system.

Long-term stability and reusability are critical factors in evaluating the PEC performance and practical applicability of photocathode materials. The operational stability of Ni/p-Si was assessed under a constant potential of -2.4 V vs. Ag/AgCl. As shown in Fig. S12, the FE for 2COOH maintained >90% of its initial value over four consecutive PEC carboxylation cycles, demonstrating excellent cycling stability of the Ni/p-Si photocathode. To further examine the structural and chemical stability of the photocathode, post-reaction characterization studies were conducted. The SEM image displayed in Fig. S13a shows that the post-carboxylation Ni/p-Si electrode retained its pristine micro-pyramidal morphology after long-term PEC operation, with the Ni catalytic sites remaining well-dispersed

across the textured silicon surface. The XRD pattern of the tested Ni/p-Si electrode revealed the appearance of distinct  $SiO_2$  diffraction peaks at  $2\theta$  =  $20.8^{\circ}$  and  $26.6^{\circ}$  (JCPDS no. 46-1045), confirming the formation of a surface oxide layer during PEC operation (Fig. S13b). The chemical states of Ni/p-Si after PEC carboxylation were measured by XPS (Fig. S14). XPS analysis confirmed that the valence state of Ni remained relatively unchanged after the long-time stability test, suggesting that the Ni catalyst was chemically stable. However, a significant increase in the  $SiO_2$  peak intensity was observed, indicating photocorrosion of the underlying silicon, which likely contributed to the slight degradation of the photoelectrocatalytic performance during extended use.  $^{46,47}$ 

The substrate scope of the PEC carboxylation protocol was systematically investigated using a range of styrene derivatives under identical reaction conditions, and the results are summarized in Fig. 5. The initial electrochemical behavior of these substrates was assessed by LSV measurements. As demonstrated in Fig. 5a, the observed reactivity trends can be explained by the electronic effect of the substituents on the C=C double bond. Styrene derivatives bearing electron-donating groups (such as methoxy, methyl, and tert-butyl substituents) showed increased electron density at the C=C bond, thereby hindering reduction and resulting in higher reduction potentials. In contrast, the derivative bearing an electron-withdrawing group (such as a trifluoromethyl substituent) exhibited decreased electron density at the C=C bond, facilitating electron acquisition and consequently displaying a positively shifted potential. Notably, trans-stilbene with an extended  $\pi$ -conjugation system showed significantly earlier onset potentials compared to unsubstituted styrene. Under optimized electrolytic potentials, the maximum FEs for PEC carboxylation of various substrates are presented in Fig. 5b. The PEC carboxylation of 4-methoxystyrene, 4-tert-butylstyrene, 4-methylstyrene, and 4-trifluoromethylstyrene produced the corresponding dicarboxylic acids with maximum FEs of 48.5%, 43.6%, 65.2%, and 52.8%, respectively, demonstrating the method's tolerance for diverse electronic substituents. In contrast, trans-stilbene preferentially underwent hydrocarboxylation with an FE of 65.8%, likely due to steric hindrance impeding the second CO<sub>2</sub> insertion.48 The synthetic utility of this PEC carboxylation strategy was further demonstrated through the preparation of pharmaceutically relevant compounds from succinic acid derivatives. Using 2-phenylsuccinic acid (2COOH, 1a) obtained via PEC carboxylation as the starting material (Fig. 5c), intramolecular Friedel-Crafts cyclization efficiently afforded compound 1aa in 90% yield. Notably, compound 1aa is a key intermediate for the synthesis of an analgesic agent. 49

To gain deeper insight into the reaction mechanism, a series of mechanistic investigations were performed. To confirm the C1 sources and elucidate the C–C bond formation mechanism, a <sup>13</sup>C labeling experiment was conducted using <sup>13</sup>CO<sub>2</sub> (Fig. 6a). The results revealed complete <sup>13</sup>C incorporation into the dicarboxylation product 1a' (Fig. S15), confirming that both carboxyl groups originated exclusively from CO<sub>2</sub>, thereby eliminating the possibility of alternative carbon

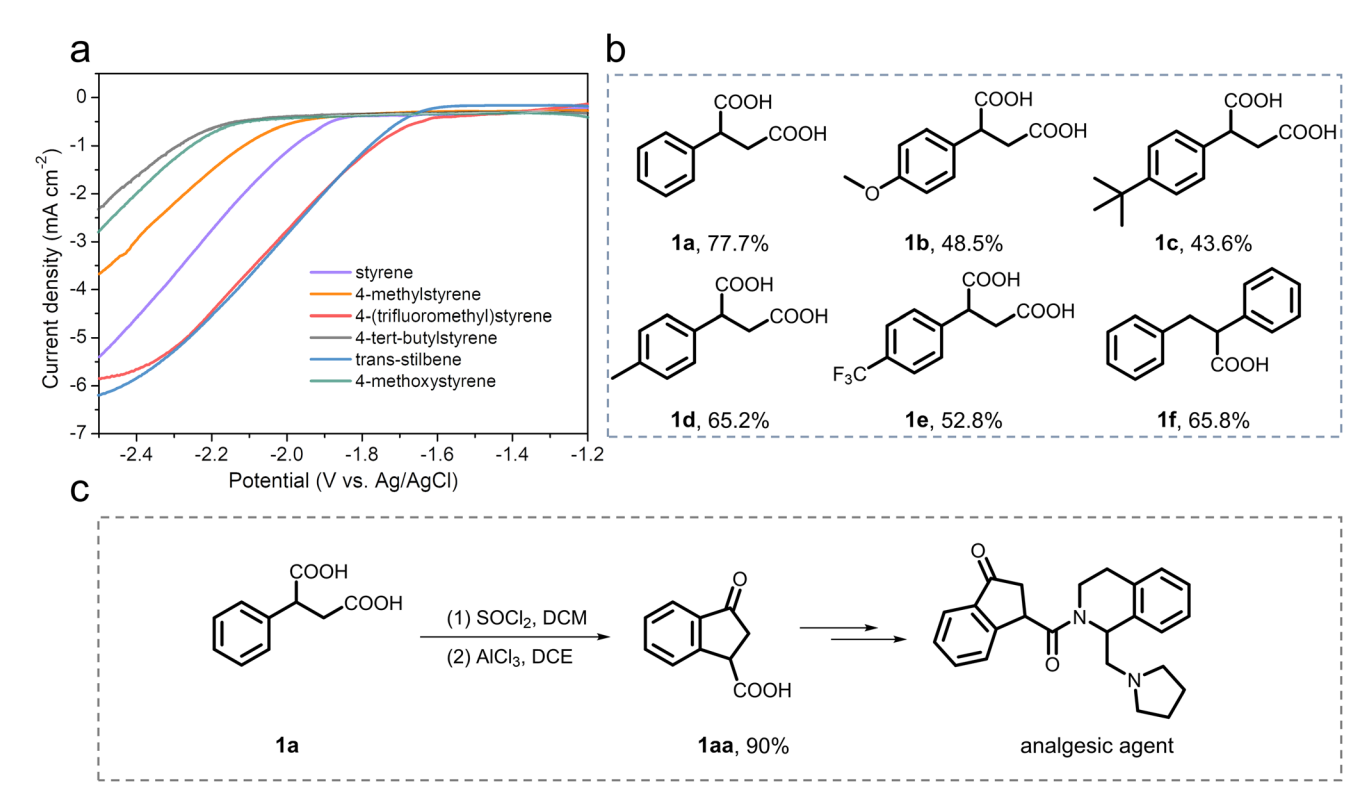


Fig. 5 Scope of styrene derivatives for PEC carboxylation. (a) LSV curves of 0.1 M styrene derivatives. (b) FEs of the products, determined by  $^{1}$ H NMR. The PEC carboxylation of styrene derivatives was conducted on the Ni/p-Si photocathode in CO<sub>2</sub>-saturated 0.1 M TBAB acetonitrile containing 0.1 M substrate. (c) Demonstration of the synthetic utility of the PEC dicarboxylation strategy.

sources contributing to the carboxylation process. Additionally, LSV revealed similar onset potentials for  $\mathrm{CO}_2$  and styrene reduction, suggesting that both reductions may occur competitively under PEC carboxylation conditions. This overlap complicates the direct identification of the initial activation step, thereby necessitating further radical-trapping and intermediate-probing experiments to clarify the mechanistic pathway.

The involvement of radical intermediates in the PEC carboxylation mechanism was supported by radical-trapping experiments. The addition of a radical scavenger (e.g., 2,2,6,6tetramethylpiperidine-1-oxyl, TEMPO) effectively suppressed the formation of the dicarboxylation product, strongly indicating that radical species are key intermediates in the reaction pathway (Fig. 6b). Meanwhile, two radical-derived adducts, designated as A and B, were identified by HPLC-APCI-TOF/MS analysis (Fig. S16), providing additional evidence for the generation of a benzylic carbanion intermediate during the reaction. Moreover, the control experiment demonstrated only trace amounts of formate (HCOO<sup>-</sup>) generation from CO<sub>2</sub> reduction in the absence of styrene (Fig. 6c and Fig. S17), further demonstrating that the initial electron transfer to CO<sub>2</sub> is less favored than electron transfer to styrene under the reaction conditions. 49 Electron paramagnetic resonance (EPR) spectroscopy further supported the reduction of styrene to generate alkyl radicals in this system (Fig. 6b Fig. S18). 51,52

Based on the above experiments, the possible mechanism for the PEC carboxylation is proposed in Fig. 6d. Upon light irradiation, the p-Si photocathode produces photogenerated electrons, which migrate to the electrode surface. These electrons are transferred to styrene and  $CO_2$ , forming a  $\beta$ -carboxylate radical intermediate through a single-electron reduction process. Subsequently, a second electron transfer converts the radical into a  $\beta$ -carboxylate carbanion intermediate. This nucleophilic intermediate can then follow two competing pathways: it either attacks a second molecule of  $CO_2$  to yield the dicarboxylated product (2COOH) or undergoes protonation to form the hydrocarboxylated product (1COOH).

In terms of product separation, the isolation of phenylsuccinic acid is straightforward despite the use of TBAB/acetonitrile solutions under dilute conditions. After the completion of the PEC carboxylation reaction, the acetonitrile solvent is first removed by rotary evaporation under reduced pressure to concentrate the reaction mixture. The concentrated solution is then acidified to convert the phenylsuccinate salt into the free phenylsuccinic acid. Due to the significantly lower solubility of phenylsuccinic acid compared to its salt form in water, the product can efficiently precipitate as a high-purity solid, enabling straightforward separation and purification *via* simple suction filtration. This simple precipitation–filtration process avoids the need for complex extraction or energy-intensive purification steps, thereby enhancing the overall sustainability of the methodology.

a. Detection of <sup>13</sup>C-involving product

**EPR** measurement

Standard conditions

c. Detection of formate

Fig. 6 Investigation of the reaction mechanism. (a)  $^{13}$ CO<sub>2</sub> labelling experiment. (b) Radical trapping experiment. (c) Detection of formate. (d) Proposed mechanism for PEC carboxylation of styrene with CO<sub>2</sub> on the Ni/p-Si photocathode.

#### Conclusion

In summary, we have developed a Ni-modified p-type micropyramid silicon (Ni/p-Si) photocathode for efficient PEC carboxylation of styrene with CO<sub>2</sub>. The Ni catalyst plays a crucial role in enhancing the PEC carboxylation performance by effectively promoting charge carrier separation and transfer while simultaneously suppressing charge recombination. The Ni/p-Si photocathode exhibits outstanding catalytic performance for PEC dicarboxylation, achieving 77.7% FE toward phenylsuccinic acid at -2.4 V vs. Ag/AgCl. The system exhibits a broad substrate scope under mild conditions without a sacrificial anode, establishing its practical applicability for sustainable dicarboxylic acid production. This work not only advances the

design of catalyst-integrated silicon photoelectrodes but also offers valuable mechanistic insights into PEC CO<sub>2</sub> fixation, contributing to the broader development of artificial photosynthetic systems for solar-to-chemical energy conversion and green organic synthesis.

### Conflicts of interest

The authors declare no competing interests.

# Data availability

The data supporting this article have been included as part of the supplementary information (SI). Supplementary information: NMR spectra of phenylsuccinic acids; SEM images, XPS, XRD and UV–vis diffuse reflectance spectra of photocathodes; HPLC chromatograms of the products; EPR and TOF LC/MS spectra of the radical trapping experiments. See DOI: https://doi.org/10.1039/d5gc03730a.

## Acknowledgements

This work was financially supported by the National Key R&D Program of China (2022YFA0911900), the National Natural Science Foundation of China (NSFC) (Grant No. 22172011 and 22088102), and the Fundamental Research Funds for the Central Universities (DUT23LAB611). This project has received funding from the European Union's Horizon 2020 research and innovation programme under the Marie Skłodowska-Curie grant agreement no. 101208839.

#### References

- 1 H. Xiao, B. Yu, S. Yan, W. Zhang, X. Li, Y. Bao, S. Luo, J. Ye and D. Yu, *Chin. J. Catal.*, 2023, **50**, 222–228.
- 2 Y. You, W. Kanna, H. Takano, H. Hayashi, S. Maeda and T. Mita, *J. Am. Chem. Soc.*, 2022, **144**, 3685–3695.
- 3 Q. Liu, L. Wu, R. Jackstell and M. Beller, *Nat. Commun.*, 2015, **6**, 5933.
- 4 P. De Luna, R. Quintero-Bermudez, C.-T. Dinh, M. B. Ross, O. S. Bushuyev, P. Todorović, T. Regier, S. O. Kelley, P. Yang and E. H. Sargent, *Nat. Catal.*, 2018, 1, 103–110.
- 5 Q. Shen, X. Huang, J. B. Liu, C. Guo and G. Zhao, *Appl. Catal.*, *B*, 2017, **201**, 70–76.
- 6 L. Lu, X. Sun, J. Ma, D. Yang, H. Wu, B. Zhang, J. Zhang and B. Han, *Angew. Chem., Int. Ed.*, 2018, 57, 14149–14153.
- 7 L. Zhang, L. P. Xiao, D. F. Niu, Y. W. Luo and J. X. Lu, Chin. J. Chem., 2008, 26, 35–38.
- 8 G. Yuan, H. Jiang and C. Lin, *Tetrahedron*, 2008, **64**, 5866–5872.
- 9 S. A. Fors, Y. J. Yap and C. A. Malapit, *Angew. Chem., Int. Ed.*, 2025, **64**, e202424865.

- 10 Y. Zhang, H. Ren, H. Zhou, P. Luo, Q. Wan, X. Zhang, B. Wang, B. Chen and B. Zhang, Molecules, 2025, 30, 40.
- 11 G. Q. Yuan, H. F. Jiang, C. Lin and S. J. Liao, *Electrochim. Acta*, 2008, 53, 2170–2176.
- 12 Y. Quan, R. Yu, J. Zhu, A. Guan, X. Lv, C. Yang, S. Li, J. Wu and G. Zheng, J. Colloid Interface Sci., 2021, 601, 378–384.
- 13 L. Song, W. Wang, J. Yue, Y. Jiang, M. Wei, H. Zhang, S. Yan, L. Liao and D. Yu, *Nat. Catal.*, 2022, 5, 832–838.
- 14 H. Seo, A. Liu and T. F. Jamison, J. Am. Chem. Soc., 2017, 139, 13969–13972.
- 15 T. Yuan, Z. Wu, S. Zhai, R. Wang, S. W. Wu, J. Cheng, M. Zheng and X. Wang, *Angew. Chem., Int. Ed.*, 2023, 62, e202304861.
- 16 P. Xu, S. Wang, H. Xu, Y. Liu, R. Li, W. Liu, X. Wang, M. Zou, Y. Zhou, D. Guo and X. Zhu, ACS Catal., 2023, 13, 2149–2155.
- 17 H. Senboku, H. Komatsu, Y. Fujimura and M. Tokuda, Synlett, 2001, 418–420.
- 18 C. Williams, J. Johnson and T. Rovis, *J. Am. Chem. Soc.*, 2008, **130**, 14936–14937.
- 19 B. Zhong, D. He, R. Chen, T. Gao, Y. Wang, H. Chen, Y. Zhang and D. Wang, *Phys. Chem. Chem. Phys.*, 2019, 21, 17517–17520.
- 20 A. Alkayal, V. Tabas, S. Montanaro, I. A. Wright, A. V. Malkov and B. R. Buckley, J. Am. Chem. Soc., 2020, 142, 1780–1785.
- 21 N. Zhang, R. Long, C. Gao and Y. Xiong, *Sci. China Mater.*, 2018, **61**, 771–805.
- 22 X. Chang, T. Wang, P. Yang, G. Zhang and J. Gong, Adv. Mater., 2019, 31, 1804710.
- 23 A. O. Ustyuzhanin, O. V. Bityukov, P. V. Sokolovskiy, V. M. Merkulova, A. I. Ilovaisky, L.-N. He, V. A. Vil' and A. O. Terent'ev, *Chem. Commun.*, 2024, 60, 8099–8102.
- 24 J. Hu, N. Fan, C. Chen, Y. Wu, Z. Wei, B. Xu, Y. Peng, M. Shen and R. Fan, Appl. Catal., B, 2023, 327, 122438.
- 25 Z. Luo, T. Wang and J. Gong, Chem. Soc. Rev., 2019, 48, 2158-2181.
- 26 K. Sun, S. Shen, Y. Liang, P. Burrows, S. Mao and D. Wang, Chem. Rev., 2014, 114, 8662–8719.
- 27 D. Zhang, J. Shi, W. Zi, P. Wang and S. Liu, *ChemSusChem*, 2017, **10**, 4324–4341.
- 28 D. Liu, J. Ma, R. Long, C. Gao and Y. Xiong, *Nano Today*, 2017, 17, 96–116.
- 29 R. Liu, G. Yuan, C. L. Joe, T. Lightburn, K. L. Tan and D. Wang, *Angew. Chem., Int. Ed.*, 2012, 51, 6709–6712.
- 30 R. Chen, K. Tian, D. He, T. Gao, G. Yang, J. Xu, H. Chen, D. Wang and Y. Zhang, ACS Appl. Energy Mater., 2020, 3, 5813–5818.
- 31 R. Liu, C. Stephani, J. Han, K. Tan and D. Wang, *Angew. Chem., Int. Ed.*, 2013, **52**, 4225–4228.
- 32 J. Yu, H. Zhang, T. Cai, W. Wang, L. Mu, G. She and W. Shi, *ACS Appl. Nano Mater.*, 2023, **6**, 821–826.
- 33 F. Li, Y. Li, Q. Zhuo, D. Zhou, Y. Zhao, Z. Zhao, X. Wu, Y. Shan and L. Sun, ACS Appl. Mater. Interfaces, 2020, 12, 11479–11488.
- 34 X. Sun, J. Jiang, Y. Yang, Y. Shan, L. Gong and M. Wang, *ACS Appl. Mater. Interfaces*, 2019, **11**, 19132–19140.

Paper

- 35 Y. Yang, M. Wang, P. Zhang, W. Wang, H. Han and L. Sun, ACS Appl. Mater. Interfaces, 2016, 8, 30143–30151.
- 36 J. Xiao, F. Long, S. Yi, H. Luo, C. Cai and H. Gong, *Green Chem.*, 2025, 27, 5764–5769.
- 37 Y. Liu, X. Li, K. Cai, L. Cai, N. Lu and J. Shi, *Appl. Soil Ecol.*, 2015, **93**, 78–87.
- 38 Y. Lu and G. Sun, J. Sep. Sci., 2020, 44, 735-743.
- 39 X. Jia, E. Stewart-Jones, J. L. Alvarez-Hernandez, G. P. Bein, J. L. Dempsey, C. L. Donley, N. Hazari, M. N. Houck, M. Li, J. M. Mayer, H. S. Nedzbala and R. E. Powers, *J. Am. Chem. Soc.*, 2024, 146, 7998–8004.
- 40 B. Shang, C. L. Rooney, D. J. Gallagher, B. T. Wang, A. Krayev, H. Shema, O. Leitner, N. J. Harmon, L. Xiao, C. Sheehan, S. R. Bottum, E. Gross, J. F. Cahoon, T. E. Mallouk and H. Wang, *Angew. Chem., Int. Ed.*, 2022, 62, e202215213.
- 41 Y. Wang, F. Li, X. Zhou, F. Yu, J. Du, L. Bai and L. Sun, *Angew. Chem., Int. Ed.*, 2017, **56**, 6911–6915.
- 42 C. Liu, F. Li, L. Wang, Z. Li, Y. Zhao, Y. Li, W. Li, Z. Zhao, K. Fan, F. Li and L. Sun, *Fundam. Res.*, 2024, 4, 291–299.
- 43 X. Long, C. Wang, S. Wei, T. Wang, J. Jin and J. Ma, ACS Appl. Mater. Interfaces, 2020, 12, 2452–2459.

- 44 B. Klahr, S. Gimenez, F. Fabregat-Santiago, J. Bisquert and T. W. Hamann, J. Am. Chem. Soc., 2012, 134, 16693–16700.
- 45 J. Zhang, R. García-Rodríguez, P. Cameron and S. Eslava, *Energy Environ. Sci.*, 2018, **11**, 2972–2984.
- 46 I. Roh, S. Yu, C. Lin, S. Louisia, S. Cestellos-Blanco and P. Yang, J. Am. Chem. Soc., 2022, 144, 8002–8006.
- 47 B. Seger, T. Pedersen, A. B. Laursen, P. Vesborg, O. Hansen and I. Chorkendorff, J. Am. Chem. Soc., 2013, 135, 1057– 1064.
- 48 Y. Zhu, X. N. Li, Z. Wen, R. Zhao, Z. Chen, Z. Zhang, H. Gao, S. Wang and F. Li, J. Am. Chem. Soc., 2024, 146, 21903–21912.
- 49 T. Ju, Y. Zhou, K. Cao, Q. Fu, J. Ye, G. Sun, X. Liu, L. Chen, L. Liao and D. Yu, *Nat. Catal.*, 2021, 4, 304–311.
- 50 Y. Kim, G. D. Park, M. Balamurugan, J. Seo, B. K. Min and K. T. Nam, *Adv. Sci.*, 2019, 7, 1900137.
- 51 B. Zhang, T. Li, Z. Mao, M. Jiang, Z. Zhang, K. Zhao, W. Qu, W. Xiao and J. Chen, *J. Am. Chem. Soc.*, 2024, **146**, 1410– 1422.
- 52 H. Huang, J. Ye, L. Zhu, C. Ran, M. Miao, W. Wang, H. Chen, W. Zhou, Y. Lan, B. Yu and D. Yu, CCS Chem., 2021, 3, 1746–1756.